ACS APPLIED MATERIALS & INTERFACES

Research Article

www.acsami.org

Fabrication of Perforated Isoporous Membranes via a Transfer-Free Strategy: Enabling High-Resolution Separation of Cells

Yang Ou,[†] Chang-Jiang Lv,[‡] Wei Yu,[†] Zheng-Wei Mao,[†] Ling-Shu Wan,*[,†] and Zhi-Kang Xu[†]

[†]MOE Key Laboratory of Macromolecular Synthesis and Functionalization, Department of Polymer Science and Engineering, and [‡]State Key Laboratory of Chemical Engineering, Department of Chemical and Biochemical Engineering, Zhejiang University, Hangzhou 310027, People's Republic of China

Supporting Information

ABSTRACT: Thin perforated membranes with ordered pores are ideal barriers for high-resolution and high-efficiency selective transport and separation of biological species. However, for self-assembled thin membranes with a thickness less than several micrometers, an additional step of transferring the membranes onto porous supports is generally required. In this article, we present a facile transfer-free strategy for fabrication of robust perforated composite membranes via the breath figure process, and for the first time, demonstrate the application of the membranes in high-resolution cell separation of yeasts and lactobacilli without external pressure, achieving almost 100% rejection of yeasts and more than 70% recovery of lactobacilli with excellent viability. The avoidance of the transfer step simplifies the fabrication procedure of composite membranes and greatly improves the membrane homogeneity. Moreover, the introduction of an elastic triblock copolymer increases the interfacial strength between the membrane and the support, and allows the preservation of composite membranes in a dry state. Such perforated ordered membranes can also be applied in other size-based separation systems, enabling new opportunities in bioseparation and biosensors.

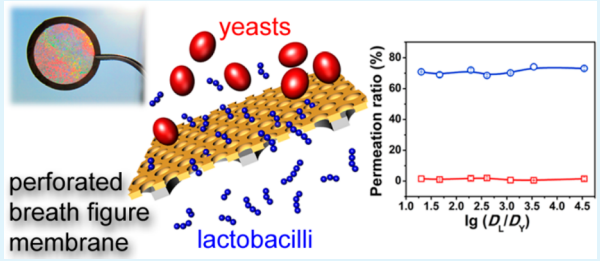

KEYWORDS: *porous materials, isoporous membranes, self-assembly, breath figures, cell separation*

1. INTRODUCTION

Cell separation is important in environmental protection, healthcare, food, and biotechnology industries, for example, yeast harvesting in beer brewing,[1] specific capture and detection of circulating tumor cells in blood,[2−5] and isolation of stem, blood, and tissue cells.[6−10] Separation of eukaryotic cells (e.g., yeasts) from prokaryotic cells (e.g., lactobacilli) is essential for the diagnosis of bacterial infections and food contaminations.[11,12] Typically, yeasts play a substantial role in the spoilage of commercial fruit yogurts fermented by lactobacillus bacteria.[11] Currently, a series of cell separation techniques have been developed,[13] among which centrifugation and membrane filtration are the most commonly used techniques. As cell separation through centrifugation is a time-consuming and labor-intensive process, membrane filtration provides a rapid, simple, energy-saving, and inexpensive method and has been widely applied to large-scale bioseparation including cell separation.[14,15] However, commonly used membranes prepared by phase inversion exhibit a high pore coefficient of variation (CV > 20%) and large thickness (typically several tens of micrometers) with tortuous pore paths, resulting in a low separation accuracy and huge flow resistance.[16] Alternatively, perforated membranes with ordered pore arrays are ideal for high-resolution and efficient biological transport and separation.[17−20]

Up to now, techniques for fabricating perforated membranes include track etching, anodization, lithographic microfabrication, and self-assembly approaches such as colloidal crystal assembly, emulsion templating, breath figures, and microphase separation of block copolymers.[16,21−24] Although track etched and anodized aluminum oxide membranes with micrometer-sized ordered pores have been commercially available, the former still suffers from low pore density (~15%) and the later is costly. Furthermore, both of the commercialized membranes have long pore channels (~15−20 μm), which are promising in single file diffusion[16−20,25] but require relatively high operation pressure. It should be noted that high operation pressure is not desirable for cell separation because of the possible viability loss of cells which are sensitive to physical stresses, and besides, high operation pressure may induce unexpected cell permeation through membranes with a pore size much smaller than the cell size because of cell deformation. Self-assembly processes offer a promising alternative to fabricate ultrathin perforated membranes, which enable not only an extra separation accuracy but also a low or ultralow operation pressure and a significant enhancement of mass transport rates.[23] For example, in a previous communication we reported an ordered membrane

Received: September 18, 2014
Accepted: November 25, 2014
Published: November 25, 2014

   dx.doi.org/10.1021/am506419z | ACS Appl. Mater. Interfaces 2014, 6, 22400−22407

prepared at an ice/air interface followed by a transfer step, which shows perfect size-selective separation of polystyrene microspheres.[26] Although Peinemann et al. has reported an integral (nontransfer) preparation of asymmetric membranes by the combination of nonsolvent-induced phase separation and self-assembly of amphiphilic block copolymers,[27−32] for self-assembled thin perforated membranes with a thickness less than several micrometers, an additional step of transferring the membranes onto porous supports is generally required.[33−36] Because of the high porosity of perforated structures and the inherent fragility of membrane materials, pore cracks may occur in the transfer process, which attenuates the separation selectivity and mechanical durability of the membranes. In addition, it is important to strengthen the interfacial adhesion between membranes and the supports so that it will be feasible to recover cells or reduce membrane fouling by back flushing. Moreover, most self-assembled membranes and even some phase inversion membranes that have a thickness of several tens of micrometers must be preserved in wet state (e.g., in glycerin) to prevent from possible pore collapse during the drying process. For cell separation, membranes need to be sterilized before use, and thus membranes that can be preserved at a dry state are highly desirable.

Here we present a facile transfer-free strategy for fabrication of robust perforated composite membranes via a self-assembly process and the application in cell separation. The transfer step is avoided in this method, which simplifies the procedure of fabricating composite membranes and greatly improves the homogeneity of the membranes; on the other hand, blending an elastic triblock copolymer further increases the interfacial adhesion strength between the membrane and the porous support. As a result of the rational design of the fabrication process as well as membrane-forming material chemistry, the composite membranes are able to be preserved in dry state and durable to back flushing. Separation of mixtures of yeasts and lactobacilli demonstrated almost 100% rejection of yeasts and more than 70% recovery of lactobacilli. The permeated lactobacilli show excellent viability, which is confirmed by cell culture experiments. We believe that this is the first example of cell separation using a thin perforated self-assembled membrane without external pressure, which can also be applied in other size-based separation systems, enabling new opportunities in bioseparation and biosensors. Moreover, the proposed transfer-free strategy provides a new pathway to prepare other composite materials.

2. EXPERIMENTAL SECTION

Materials. The synthesis of polystyrene-*block*-poly(*N*,*N*-dimethylaminoethyl methacrylate) (PS_{247}-*b*-$PDMAEMA_{14}$, M_n = 27 900 g mol^{-1}, M_w/M_n = 1.24) by atom transfer radical polymerization was described elsewhere.[37] Polystyrene-*block*-polyisoprene-*block*-polystyrene (SIS, 22 wt % styrene, M_n = 158600 g mol^{-1}, M_w/M_n = 1.18) was purchased from Sigma-Aldrich and used as received. Transmission electron microscopy (TEM) grids (Φ12 mm) were purchased from Beijing Xinxing Braim Technology Co. Ltd. (China) and used as porous supports. Before used, the TEM grids were sonicated with acetone for 15 min and blow-dried by nitrogen gas. Poly(ethylene terephthalate) (PET) films were kindly provided by Hangzhou Tape Factory (China) and cleaned with acetone for 5 min and repeated three times before used. The yeast strains, *Saccharomyces cerevisiae* (*S. cerevisiae*), were purchased from Zhejiang Microbiology Institute (China). The lactobacillus strains, *Streptococcus thermophilus* (*S. thermophilus*), were purchased from China Center of Industrial Culture Collection. Water used in the experiments was deionized and ultrafiltrated to 18.2 MΩ with an ELGA LabWater system. All other reagents were acquired from Sinopharm Chemical Reagent Co. Ltd. (China) and used without further purification.

Transfer-Free Fabrication Method. Perforated honeycomb composite membranes were prepared at an air/ice interface according to the following procedure.[26] Typically, a cleaned TEM grid was placed in a PS Petri dish (Φ 30 mm) and covered by a thin ice layer with a thickness of ∼1 mm. Then, a solution of PS_{247}-*b*-$PDMAEMA_{14}$/SIS (40 μL) in carbon disulfide (CS_2) was drop-cast onto the surface of ice well above the TEM grid under a humid airflow at room temperature. The concentration of PS_{247}-*b*-$PDMAEMA_{14}$ was fixed at 1 mg mL^{-1} while the SIS weight fraction in the blends varied from 0 to 80 wt %. The relative humidity of the airflow, measured by a hygrothermograph (DT-321S, CEM Corporation), was maintained around 80% by bubbling through distilled water, and the flow rate was controlled via a needle valve and measured by a flow meter. A thin turbid solution film formed on the ice/water surface in merely several seconds. As the evaporation of CS_2 and condensed water droplets, the thin ice layer above the TEM grid gradually melted into water and infiltrated down through the wide openings of the grid, which leads to self-adhesion of the honeycomb membrane onto the TEM grid. Consequently, a composite membrane was directly fabricated without further membrane transfer steps in only several minutes. To prevent the honeycomb membrane from unexpected cracking induced by the capillary force during water evaporation, we immersed the as-prepared composite membrane in ethanol for 10 s to completely replace the water remaining in the pores before drying in the air at room temperature. The composite membranes in the dry state could be stored well with no obvious cracks for more than 30 days.

Membrane Characterizations. The integrity and interfacial adhesion strength of the honeycomb membranes were assessed by microscope images obtained from an optical microscopy (Ti−U, Nikon). The integrity ratio, *I*, is defined as the ratio of TEM grid area covered by honeycomb membranes with none-cracking pores (S_H) to the whole TEM grid dimension (S_T), which is given as

$$I = \frac{S_H}{S_T} \times 100\%$$

The average integrity ratio is obtained from 5 parallel pieces of composite membranes and the integrity of each membrane is calculated from 3 random locations.

The assessment of interfacial adhesion strength is borrowed from the method for evaluating paint adhesion force. Perforated honeycomb membranes transferred on PET films were prepared and pressed by an adhesive Scotch tape onto the membrane surface. The adhesion ratio, *A*, is defined as the ratio of residual area of membranes after the unfirm pore structures were peeled off from the support (S_R) to the whole PET film dimension (S_P), which is given as

$$A = \frac{S_R}{S_P} \times 100\%$$

The average adhesion ratio is obtained from 5 parallel pieces of honeycomb membranes on PET films and the adhesion strength of each membrane is calculated from 3 random locations.

The pore diameter distribution of the honeycomb membranes was statistically analyzed by measuring the pore sizes of over 100 pores on the top and bottom surface through the corresponding SEM images, respectively.

Cell Separation Assay. A honeycomb composite membrane with a diameter of 12 mm was mounted in a homemade permeation module. Before filtration, the composite membrane was sterilized in 75% alcohol for 10 min and rinsed by physiological saline three times to completely replace the air captured in the pores and wet the membrane surface. Yeasts and lactobacilli were mixed and dispersed in physiological saline with various cell densities. The separation was performed in a dead-end mode without any additional pressure. The feed cell dispersion was flowed through the filter chamber and the filtrate was collected in a 10 mL vial for subsequent characterization. The cell separation process was recorded by a real-time monitoring

optical video (see the Supporting Information, Movie S1: yeast filtration, the yeast cell density in the feed solution is 3.4×10^6 cfu mL^{-1}; Movie S2: separation of mixtures of yeasts and lactobacilli, the cell density of yeasts and lactobacilli in the feed solution was 3.4×10^6 and 6.8×10^7 cfu mL^{-1}, respectively). On the other hand, the sterilization and rinsing process were the same for the sucking filtration method. The feed solution of yeast cells in a vial was sucked up into the syringe at a speed of about 0.25 mL min^{-1}. The permeation ratio of a specific type of cells is defined as the proportion of the cell density in the filtrate solution to that in the feed.

The cell density of yeasts and lactobacilli was obtained by cell counting via a hemocytometer and from OD600 values by an UV−vis spectrophotometer (UV-2450, Shimadzu), respectively. The relationship between the cell density and OD600 values of yeasts was determined by the results of cell counting and UV adsorption value, giving the yeast cell density of 1.46×10^7 cfu mL^{-1} at OD600 = 1.0. The relationship between the cell density and OD600 values of lactobacilli was established according to the National food safety standard food microbiological examination (GB 4789.35−2010), which shows the lactobacillus cell density of 3.89×10^8 cfu mL^{-1} at OD600 = 1.0.

3. RESULTS AND DISCUSSION

Transfer-Free Membrane Fabrication. Inspired by water droplet arrays condensed on cold substrates, the breath figure technique provides a simple, robust, and efficient strategy to fabricate honeycomb membranes with a pore size range of submicrometer to tens of microns.[38−47] As pioneered by Parisi and co-workers,[48] honeycomb membranes with perforated pore structures were successfully prepared via depositing a dilute polymer solution on liquid surface with an adequately large surface tension (e.g., water).[26,49−55] We originally demonstrated the use of ice as the substrate for preparing perforated honeycomb membranes.[26] Traditionally, a polymer solution is cast onto water or ice surface with a dimension and thickness far beyond that of the resultant honeycomb membrane,[26,49−55] and the as-prepared membrane will be finally floating on water surface. Then, the membrane can be carefully transferred to supports. In theory, only the outermost surface layer of the substrate (e.g., water) is essential to the formation of perforated membranes.[26] Obviously, a membrane would spontaneously adhere to the support on a lowering water surface.[56] Hence, it is possible to prepare perforated honeycomb membranes on a thin ice layer without further transfer steps. Typically, porous supports, such as TEM grids, were placed in a PS Petri dish (Φ 30 mm) and covered by a thin ice layer with a thickness of ∼1 mm (Figure 1a). A solution of PS-*b*-PDMAEMA/SIS blends in

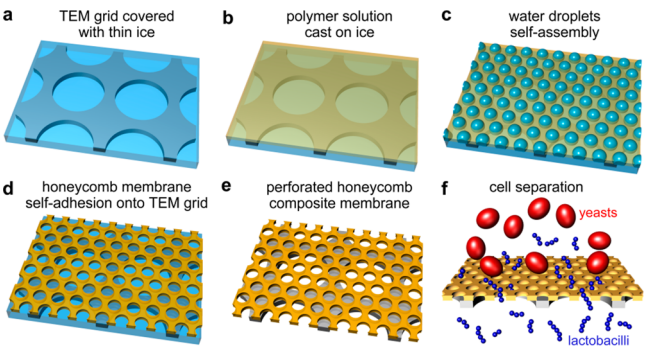

Figure 1. Schematic illustrations of the fabrication of perforated honeycomb membranes on porous supports such as TEM grids via (a−e) a transfer-free breath figure method and (f) the cell separation process.

CS_2 was drop-cast onto the air/ice interface well above the TEM grid under a humid airflow with ∼80% relative humidity (Figure 1b). The polymer solution would spread at the air/ice interface, resulting in a thin, disk-like, turbid solution film on the ice/water surface in merely several seconds. The diameter of the solution film was about 17 mm, which is slightly larger than that of a TEM grid. Condensed water droplets induced by evaporative cooling self-assemble into hexagonal arrays as a result of Marangoni convection and thermocapillary force, and penetrate the polymer solution film induced by the excess of the surface tension differential pressure to the critical rupture pressure across the pores (Figure 1c).[26] As the evaporation of CS_2 and water, the thin ice layer above the TEM grid gradually melts into water and infiltrates down through the wide openings of the grid, leading to self-adhesion of the membrane onto the underlying TEM grid (Figure 1d). Consequently, a composite membrane can be directly fabricated without membrane transfer steps in only several minutes (Figure 1e).

A typical perforated honeycomb composite membrane is shown in Figure 2a−f. By using PS-*b*-PDMAEMA/SIS (60 wt % SIS) blends as the membrane-forming material, perforated honeycomb membranes without pore cracks in a large area were obtained via the transfer-free method. Typically, the membrane has a pore diameter of 2.5 μm on the top surface (Figure 2a, b) and 2.7 μm at the bottom (Figure 2c, d). It is noteworthy that, compared to other self-assembled membranes, the pore size of the perforated honeycomb membranes is in the micrometer range, which is well-suited for cell separation. Meanwhile, the membrane presents a considerably high porosity of up to 70% within a single opening of the TEM grid support, and a thin membrane thickness of about 2 μm (Figure 2e and Supporting Information, Figure S1e). Besides the TEM grid, other porous supports such as stainless steel sieves, nylon fabrics, and nanofibrous meshes can also be used. Moreover, it should be emphasized that we prepared highly uniform honeycomb membranes with a remarkably low pore CV down to 3.85% on both the top and bottom surface (Figure 2g). The composite membrane displays uniform bright iridescent colors when viewed with a reflected light (Figure 2f), indicating the formation of a perfectly ordered honeycomb composite filter with a membrane diameter of 12 mm (more than 1.1 cm^2, inset of Figure 2f). Generally, the maximum membrane area could be up to several square centimeters, which depends on the volume of the casting solution and the scale of supports. The high homogeneity, perfectly perforated structure, high porosity, and thin thickness may endow the membrane with high-resolution separation ability at ultralow operation pressure.

Compared to other fabrication techniques for perforated polymeric membranes with ordered pores, such as track etching, photolithography, colloidal crystal templating, and microphase separation of block copolymers, this transfer-free breath figure method allows the formation of relatively large-area membranes in a simple and time-saving way. Besides, water is utilized as templates in this method, which is nontoxic and easily available, and more interestingly, can thoroughly evaporate during the membrane formation process. As a result, an extra step for template removal is avoided.

Enhancement of Membrane Mechanical Properties. Polystyrene-based amphiphilic diblock copolymers (e.g., PS-*b*-PDMAEMA) are good candidates for membrane formation.[26,55] However, it is known that polystyrene films are fragile, especially for those films with highly porous structures.

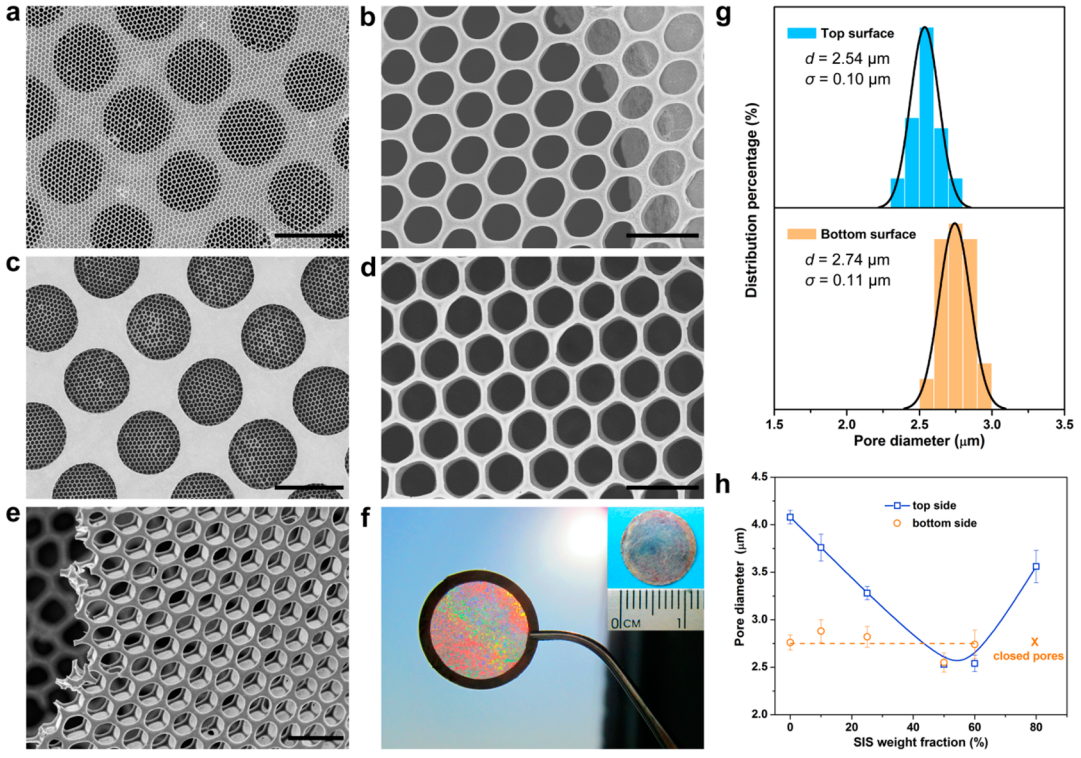

Figure 2. (a–e) SEM images of a typical perforated honeycomb composite membrane prepared by the transfer-free method from a blend of PS-*b*-PDMAEMA/SIS (60 wt % SIS). (a, b) Top side, (c, d) bottom side, and (e) cross-section. (f) Digital photographs of the composite membrane, the inset shows the actual dimension of the membrane. Scale bars: (a, c) 50 μm and (b, d, e) 5 μm. (g) Average pore diameter (d) of the top and bottom surfaces of a typical perforated honeycomb composite membrane prepared by the transfer-free method from a blend of PS-*b*-PDMAEMA/SIS (60 wt % SIS), and the corresponding standard deviations (σ). (h) Effects of SIS weight fractions in PS-*b*-PDMAEMA/SIS blends on the pore diameter.

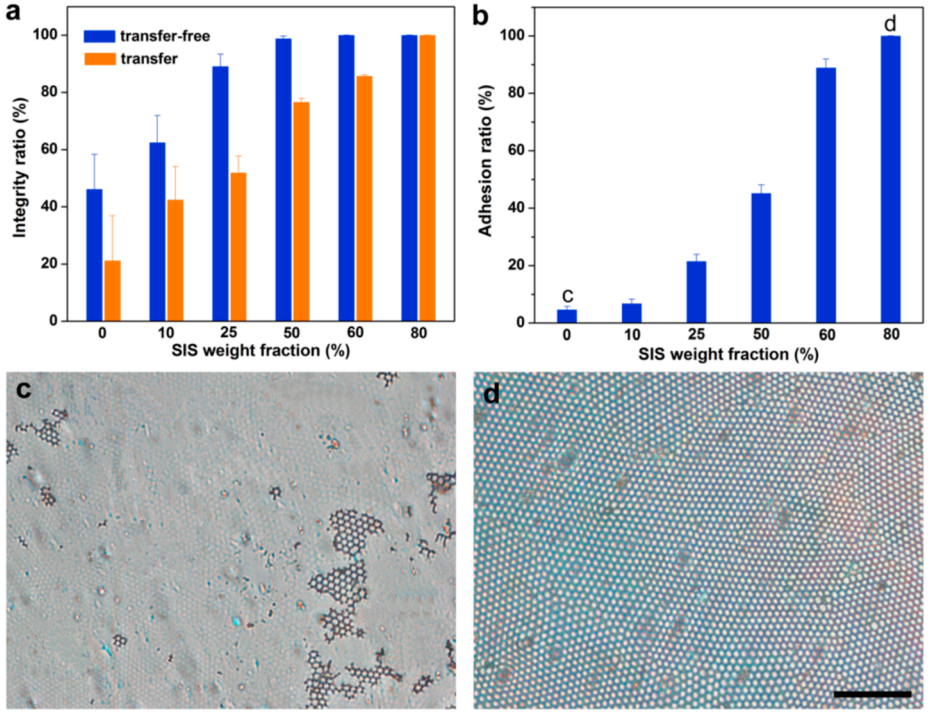

Figure 3. Membrane integrity and interfacial adhesion strength. (a, b) Effects of SIS weight fractions in PS-*b*-PDMAEMA/SIS blends on (a) the integrity and (b) the interfacial adhesion strength of the honeycomb membranes. (c, d) Typical optical images of residual pore structures of honeycomb membranes on supports after peeled off by a Scotch tape. (c) PS-*b*-PDMAEMA membrane and (d) PS-*b*-PDMAEMA/SIS blend (80 wt % SIS) membrane. Scale bar: 50 μm.

dx.doi.org/10.1021/am506419z | *ACS Appl. Mater. Interfaces* 2014, 6, 22400–22407

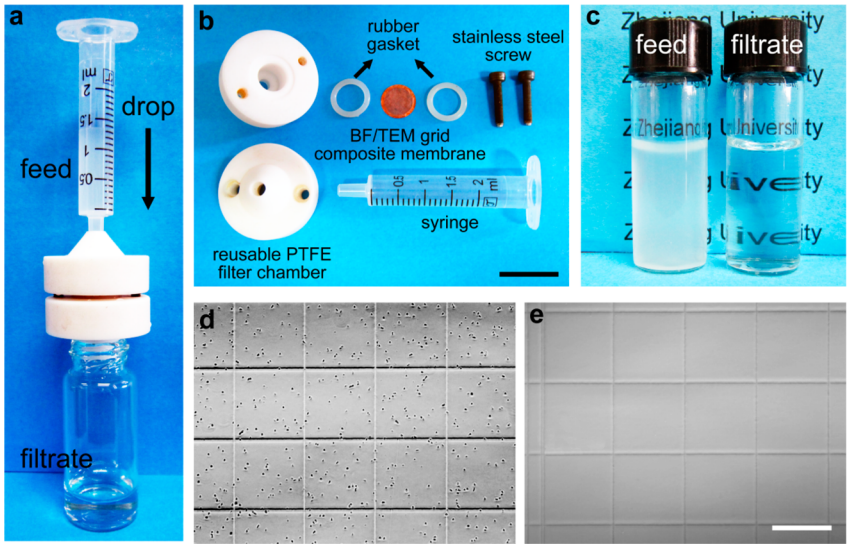

Figure 4. Yeast filtration. Digital photographs of (a) a typical yeast cell filtration process, (b) the membrane module used for cell separation, and (c) the feed and filtrate solutions. (d, e) Optical images of the (d) feed and (e) filtrate solutions on a hemocytometer. The feed solution in (a, c, d) has a yeast cell density of 3.4×10^6 cfu mL^{-1} (OD600 = 0.233) and the OD600 value of the filtrate is 0.001. Scale bars: (b) 20 mm and (d, e) 200 μm.

SIS is a commercially available elastomer and has been well demonstrated as an ideal material for constructing robust honeycomb films on nonplanar substrates.[57−59] Therefore, blends of PS-*b*-PDMAEMA and SIS with different compositions were investigated for the enhancement of membrane integrity and interfacial adhesion as well as pore structure control. As indicated in Figure 2h, the diameter of top surface pores of PS-*b*-PDMAEMA/SIS membranes can be tuned from 4.1 to 2.5 μm by changing the SIS weight fractions from 0 to 80 wt %, whereas the bottom pore size remains constant at about 2.7 μm, and dead-end pore structures are obtained at a high SIS ratio of 80 wt % (see the Supporting Information, Figures S2, S3). Besides, membranes containing 80 wt % SIS are sensitive to stretching and compressing, resulting in unstable and deformable pore structures at room temperature. A detailed discussion on the breath figure process for the formation of PS-*b*-PDMAEMA/SIS membranes can be found elsewhere (Supporting Information, breath figure process of PS-*b*-PDMAEMA/SIS membranes section and Figures S1−S7). Compared to the traditional transfer method, the integrity of the perforated honeycomb membranes has been significantly enhanced because of both the transfer-free method and the blending of elastic SIS (Figure 3a). Defects in the honeycomb composite membranes were evaluated through optical microscopy. The integrity ratio, which is the areal fraction of TEM grids covered by none-cracking honeycomb membranes increases with the weight fraction of SIS in the blends, and membranes prepared by the transfer-free method have obviously higher integrity ratios than those by the transfer method. Perforated honeycomb membranes with no cracks were obtained via the transfer-free method when the SIS weight fraction reaches 60%, whereas more than 15% area of the membrane prepared by the transfer method is still fractured (see the Supporting Information, Figures S8, S9). The elastic SIS can act as the strengthening phase in the as-prepared honeycomb membranes to protect pore structures from unexpected cracking in the self-adhesion, membrane drying, or separation processes.

The introduction of SIS can also enhance the adhesion strength between the honeycomb membrane and the porous support. Insufficient adhesion to supports leads to detachment of membranes from the supports,[55] which would obviously weaken or even eliminate the separation selectivity of the membranes. As far as we know, a direct and accurate measurement of the adhesion force of a thin polymeric membrane to a porous support is rather difficult. We evaluated the adhesion strength in a way that is borrowed from the evaluation of paint adhesion force. Perforated honeycomb membranes on supports were pressed by an adhesive Scotch tape onto the membrane surface. The adhesion strength is indicated via the adhesion ratio, which is defined as the ratio of the residual area to the whole area of membranes. As shown in Figure 3b, the adhesion ratio increases with the SIS fraction in the blends. The adhesion ratio of the membrane with 60 wt % SIS is nearly 20 times higher than that of the PS-*b*-PDMAEMA membrane. Figure 3c, d shows optical images of residual membranes with 0 and 80 wt % SIS, respectively. Almost all pore structures were removed from supports in the PS-*b*-PDMAEMA membranes, while the apparent membrane morphology in the membranes with 80 wt % SIS remains intact. Other typical images are shown in Figure S10 (Supporting Information). It can be concluded that the interfacial adhesion strength has been greatly improved by the introduction of elastic SIS. As a result of the improvement in membrane integrity and interfacial adhesion strength, the composite membrane can be preserved in dry state, unlike membranes reported previously that must be kept in wet state.[33−36] Membranes in the dry state are greatly beneficial for large scale production and practical applications.

Cell Separation. The honeycomb composite membranes were first applied to the filtration of yeast cells to evaluate the retention capability (Figure 4), which may provide a rapid and effective method to capture, enrich and even detect rare cells with ultralow concentration in a solution, e.g., *Cryptosporidium parvum* oocysts in the drinking water supply system[60] and circulating tumor cells in bloodstream.[61] The composite membrane with an outer diameter of 12 mm was mounted in a homemade permeation module, which consists of a syringe for holding the feedstock, a reusable polytetrafluoroethylene (PTFE) filter chamber, and rubber gaskets and stainless steel

screws for membrane fixing and sealing (Figure 4b). This modified module could protect the composite membranes from possible damages in the mounting process and enable a working diameter of 8 mm. Yeast cells (*S. cerevisiae*) were dispersed in physiological saline with various cell densities from 3.2×10^5 to 3.4×10^6 cfu mL^{-1}, and the filtration was performed in a dead-end mode. It is noteworthy that the filtration could be carried out without external pressure, compared to the traditional microfiltration processes where 0.1 MPa or higher pressure is necessarily applied. The feed solution flowed through the filter chamber and the filtrate was collected for subsequent cell counting. This filtration process was recorded by a real-time monitoring optical video (see the Supporting Information, Movie S1). As expected, the filtration flux of the composite filters decreased with yeast cell density, and at least a flux of 3.0×10^2 L m^{-2} h^{-1} was achieved for a yeast cell density of 3.4×10^6 cfu mL^{-1}. Figure 4c–e shows typical digital photographs and cell counting results before and after the filtration by the membrane. The feed solution displayed a yeast cell density of 3.4×10^6 cfu mL^{-1} (OD600 = 0.233), whereas the filtrate showed nearly zero yeast cells (OD600 = 0.001). The filtration results demonstrated that almost 100% yeast cells were removed from the feed solution and a clear filtrate was obtained, which indicates perfect retention to cells with a larger size than the pore diameter. The excellent retention ability of the composite membranes stems from a narrow pore size distribution of the honeycomb membranes and an ultralow operation pressure of only several centimeters water. In addition, the filtration of yeast cells could also be performed via a sucking method (Figure 5). By carefully

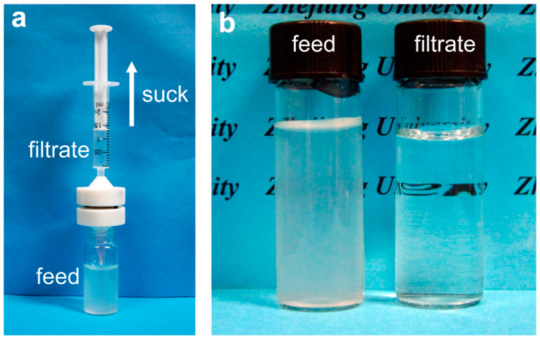

Figure 5. Digital photographs of (a) a typical yeast cell filtration via the sucking method and (b) the feed and filtrate solutions. The feed solution has a yeast cell density of 3.4×10^6 cfu mL^{-1} (OD600 = 0.233) and the OD600 value of the filtrate is 0.002.

sucking the feed solution (OD600 = 0.233) in a vial into the syringe through a stainless steel needle, yeast cells would first pass through the porous supports and then be rejected by the honeycomb membranes, resulting in a clear filtrate solution (OD600 = 0.002) collected in the syringe (Figure 5b). The successful retention of yeast cells by this sucking method further indicates the improvement of the interfacial adhesion strength between the honeycomb membrane and the porous support, and the promising back flushing ability of the composite membranes.

Subsequently, the separation of cell mixtures of yeasts and lactobacilli (*S. thermophilus*) was investigated (Figure 6 and Supporting Information, Movie S2). It is known that the *S. cerevisiae* are elliptical cells with an average minor axis diameter of 3.1 μm and the *S. thermophilus* are spherical cells with an

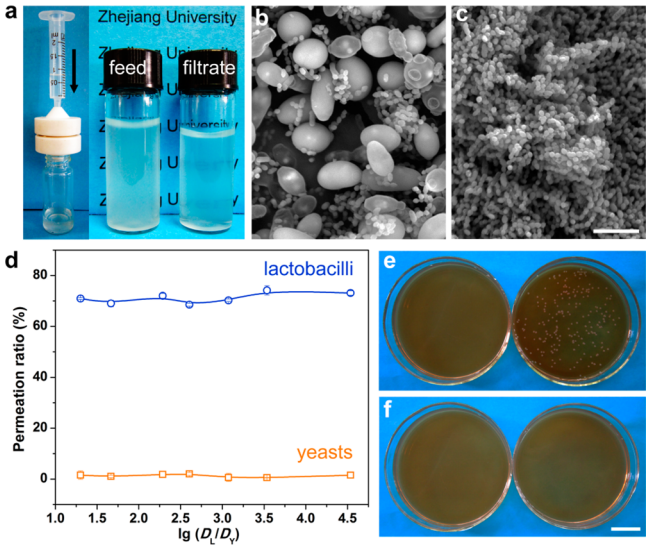

Figure 6. Cell separation. (a) Digital photographs of a typical separation process of the mixture of yeasts and lactobacilli, and the feed and filtrate solutions. (b, c) Typical SEM images of cells in the (b) feed and (c) filtrate solutions. The cell density of yeasts and lactobacilli in the feed solution was 3.4×10^6 and 6.8×10^7 cfu mL^{-1}, respectively. (d) Permeation ratios of yeasts and lactobacilli in the cell separation via the honeycomb composite membranes. (e, f) Digital photographs of the recultured filtrate solution in a lactobacillus growing medium (e) and yeast growing medium with 10 μg mL^{-1} erythromycin (f). The left culturing dishes in e and f were blank media as controls. Scale bars: (b, c) 5 μm and (e, f) 20 mm.

average diameter of 0.7 μm. Yeasts and lactobacilli were mixed and dispersed in physiological saline with various cell densities. The yeast density (D_Y) varied from 3.2×10^4 to 3.4×10^6 cfu mL^{-1} while the lactobacillus density (D_L) decreased from to 1.1×10^9 to 6.8×10^7 cfu mL^{-1}. The filtrate is still turbid because of the existence of lactobacilli although it seems slightly clearer than that of the feedstock of cell mixtures (Figure 6a). Figure 6b shows a typical SEM image of the mixed cells. As expected, yeast cells in the feed solution were almost completely retained by the aperture sieving effect of the honeycomb membranes, resulting in a permeation ratio of nearly zero (Figure 6d). Only lactobacilli can be observed from the SEM image of the filtrate (Figure 6c). Although several lactobacillus cells could link together to form a chain-like joint structure (Figure 6b) and enlarge the cell size, more than 70% of lactobacillus recovery was obtained in the filtrate (Figure 6d). The proportion of lactobacillus cells was observed to be significantly reduced in the filter residue (Supporting Information, Figure S11) as compared to that in the initial feed solution shown in Figure 6b. The filtration flux of cell mixtures is $\sim 2.6 \times 10^2$ L m^{-2} h^{-1}, which is slightly lower than that of the single solution of yeasts ($\sim 3.0 \times 10^2$ L m^{-2} h^{-1}).

The diluted filtrate solution was recultured in a lactobacilli growing medium. The permeated lactobacillus cells show an excellent viability due to the free passage through the honeycomb composite membranes under an ultralow operation pressure (Figure 6e). It is important to perform cell separation at a low transmembrane pressure. For example, in the leukocyte depletion of blood, hemolysis would occur and leukocytes could be deformed and pushed through the pores under high pressures. Meanwhile, a yeast growing medium with 10 μg mL^{-1} erythromycin as the antibiotics was also used for

reculturing the filtrate cells. As a result of the addition of erythromycin, the growth of lactobacillus cells would be completely suppressed without disturbing the breeding of yeast cells. The culturing results further indicate complete removal of yeast cells in the filtrate solution (Figure 6f). These results are consistent with those of yeast filtration shown in Figure 4 and 5. Therefore, it can be concluded that the perforated honeycomb composite membranes provide a high-resolution and energy-saving cell separation process.

4. CONCLUSION

In conclusion, we present a facile transfer-free strategy for the fabrication of robust perforated composite membranes with ordered and uniform pores. The strategy simplifies the procedures of fabricating composite membranes and greatly improves the homogeneity and interfacial adhesion strength of the membranes, enabling membranes that can be preserved in dry state and durable to back flushing. We demonstrated for the first time the use of a thin perforated membrane in high-resolution and energy-saving size-selective cell separation of yeasts and lactobacilli without external pressure. Almost 100% rejection of yeasts and more than 70% recovery of lactobacilli have been achieved by using a honeycomb membrane with an average pore diameter of 2.5 μm. In addition, the permeated lactobacilli show an excellent viability. This promising cell separation material may also be applied in other size-based separation systems, such as capture and detection of circulating tumor cells.

■ ASSOCIATED CONTENT

Supporting Information

Details of materials, instruments and characterization, the transfer fabrication method, membrane morphologies, solution viscosity, and surface chemistry analysis of membranes. This material is available free of charge via the Internet at http://pubs.acs.org.

■ AUTHOR INFORMATION

Corresponding Author

*E-mail: lswan@zju.edu.cn.

Notes

The authors declare no competing financial interest.

■ ACKNOWLEDGMENTS

This work is financially supported by the National Natural Science Foundation of China (Grants 51173161 and 21374100) and partially supported by the State Key Laboratory of Materials-Oriented Chemical Engineering (KL13-11).

■ REFERENCES

(1) Baker, R. W. *Membrane Technology and Applications*, 2nd ed.; John Wiley & Sons: New York, 2004.

(2) Adams, A. A.; Okagbare, P. I.; Feng, J.; Hupert, M. L.; Patterson, D.; Gottert, J.; McCarley, R. L.; Nikitopoulos, D.; Murphy, M. C.; Soper, S. A. Highly Efficient Circulating Tumor Cell Isolation from Whole Blood and Label-Free Enumeration Using Polymer-Based Microfluidics with an Integrated Conductivity Sensor. *J. Am. Chem. Soc.* **2008**, *130*, 8633−8641.

(3) Kaittanis, C.; Santra, S.; Perez, J. M. Role of Nanoparticle Valency in the Nondestructive Magnetic-Relaxation-Mediated Detection and Magnetic Isolation of Cells in Complex Media. *J. Am. Chem. Soc.* **2009**, *131*, 12780−12791.

(4) Wang, Y. Y.; Zhou, F.; Liu, X. L.; Yuan, L.; Li, D.; Wang, Y. W.; Chen, H. Aptamer-Modified Micro/Nanostructured Surfaces: Efficient Capture of Ramos Cells in Serum Environment. *ACS Appl. Mater. Interfaces* **2013**, *5*, 3816−3823.

(5) Zhang, P. H.; Cao, J. T.; Min, Q. H.; Zhu, J. J. Multi-Shell Structured Fluorescent-Magnetic Nanoprobe for Target Cell Imaging and on-Chip Sorting. *ACS Appl. Mater. Interfaces* **2013**, *5*, 7417−7424.

(6) Notta, F.; Doulatov, S.; Laurenti, E.; Poeppl, A.; Jurisica, I.; Dick, J. E. Isolation of Single Human Hematopoietic Stem Cells Capable of Long-Term Multilineage Engraftment. *Science* **2011**, *333*, 218−221.

(7) Drukker, M.; Tang, C.; Ardehali, R.; Rinkevich, Y.; Seita, J.; Lee, A. S.; Mosley, A. R.; Weissman, I. L.; Soen, Y. Isolation of Primitive Endoderm, Mesoderm, Vascular Endothelial and Trophoblast Progenitors from Human Pluripotent Stem Cells. *Nat. Biotechnol.* **2012**, *30*, 531−542.

(8) Kumamaru, H.; Ohkawa, Y.; Saiwai, H.; Yamada, H.; Kubota, K.; Kobayakawa, K.; Akashi, K.; Okano, H.; Iwamoto, Y.; Okada, S. Direct Isolation and Rna-Seq Reveal Environment-Dependent Properties of Engrafted Neural Stem/Progenitor Cells. *Nat. Commun.* **2012**, *3*, 1140.

(9) Avci, F. Y.; Li, X. M.; Tsuji, M.; Kasper, D. L. Isolation of Carbohydrate-Specific Cd4(+) T Cell Clones from Mice after Stimulation by Two Model Glycoconjugate Vaccines. *Nat. Protoc.* **2012**, *7*, 2180−2192.

(10) Yang, R. F.; Zheng, Y.; Burrows, M.; Liu, S. J.; Wei, Z.; Nace, A.; Guo, W.; Kumar, S.; Cotsarelis, G.; Xu, X. W. Generation of Folliculogenic Human Epithelial Stem Cells from Induced Pluripotent Stem Cells. *Nat. Commun.* **2014**, *5*, 3071.

(11) Griffiths, M. W. *Improving the Safety and Quality of Milk, Vol. 1: Milk Production and Processing*; Woodhead Publishing: Cambridge, U.K., 2010.

(12) Chrimes, A. F.; Khoshmanesh, K.; Stoddart, P. R.; Mitchell, A.; Kalantar-zadeh, K. Microfluidics and Raman Microscopy: Current Applications and Future Challenges. *Chem. Soc. Rev.* **2013**, *42*, 5880−5906.

(13) Tiwari, A.; Ramalingam, M.; Kobayashi, H.; Turner, A. P. F. *Biomedical Materials and Diagnostic Devices*; John Wiley & Sons: New York, 2012.

(14) He, D.; Susanto, H.; Ulbricht, M. Photo-Irradiation for Preparation, Modification and Stimulation of Polymeric Membranes. *Prog. Polym. Sci.* **2009**, *34*, 62−98.

(15) Yang, R.; Jang, H.; Stocker, R.; Gleason, K. K. Synergistic Prevention of Biofouling in Seawater Desalination by Zwitterionic Surfaces and Low-Level Chlorination. *Adv. Mater.* **2014**, *26*, 1711−1718.

(16) Warkiani, M. E.; Bhagat, A. A. S.; Khoo, B. L.; Han, J.; Lim, C. T.; Gong, H. Q.; Fane, A. G. Isoporous Micro/Nanoengineered Membranes. *ACS Nano* **2013**, *7*, 1882−1904.

(17) Wei, Q. H.; Bechinger, C.; Leiderer, P. Single-File Diffusion of Colloids in One-Dimensional Channels. *Science* **2000**, *287*, 625−627.

(18) Striemer, C. C.; Gaborski, T. R.; McGrath, J. L.; Fauchet, P. M. Charge- and Size-Based Separation of Macromolecules Using Ultrathin Silicon Membranes. *Nature* **2007**, *445*, 749−753.

(19) Dekker, C. Solid-State Nanopores. *Nat. Nanotechnol.* **2007**, *2*, 209−215.

(20) Zavala-Rivera, P.; Channon, K.; Nguyen, V.; Sivaniah, E.; Kabra, D.; Friend, R. H.; Nataraj, S. K.; Al-Muhtaseb, S. A.; Hexemer, A.; Calvo, M. E.; Miguez, H. Collective Osmotic Shock in Ordered Materials. *Nat. Mater.* **2012**, *11*, 53−57.

(21) Wang, Y.; Li, F. An Emerging Pore-Making Strategy: Confined Swelling-Induced Pore Generation in Block Copolymer Materials. *Adv. Mater.* **2011**, *23*, 2134−2148.

(22) Wu, D. C.; Xu, F.; Sun, B.; Fu, R. W.; He, H. K.; Matyjaszewski, K. Design and Preparation of Porous Polymers. *Chem. Rev.* **2012**, *112*, 3959−4015.

(23) van Rijn, P.; Tutus, M.; Kathrein, C.; Zhu, L.; Wessling, M.; Schwaneberg, U.; Boker, A. Challenges and Advances in the Field of Self-Assembled Membranes. *Chem. Soc. Rev.* **2013**, *42*, 6578−6592.

(24) Zhao, H.; Gu, W.; Thielke, M. W.; Sterner, E.; Tsai, T.; Russell, T. P.; Coughlin, E. B.; Theato, P. Functionalized Nanoporous Thin

Films and Fibers from Photocleavable Block Copolymers Featuring Activated Esters. *Macromolecules* **2013**, *46*, 5195−5201.
(25) Lee, W.; Ji, R.; Gosele, U.; Nielsch, K. Fast Fabrication of Long-Range Ordered Porous Alumina Membranes by Hard Anodization. *Nat. Mater.* **2006**, *5*, 741−747.
(26) Wan, L. S.; Li, J. W.; Ke, B. B.; Xu, Z. K. Ordered Microporous Membranes Templated by Breath Figures for Size-Selective Separation. *J. Am. Chem. Soc.* **2012**, *134*, 95−98.
(27) Peinemann, K. V.; Abetz, V.; Simon, P. F. Asymmetric Superstructure Formed in a Block Copolymer via Phase Separation. *Nat. Mater.* **2007**, *6*, 992−996.
(28) Nunes, S. P.; Sougrat, R.; Hooghan, B.; Anjum, D. H.; Behzad, A. R.; Zhao, L.; Pradeep, N.; Pinnau, I.; Vainio, U.; Peinemann, K. V. Ultraporous Films with Uniform Nanochannels by Block Copolymer Micelles Assembly. *Macromolecules* **2010**, *43*, 8079−8085.
(29) Nunes, S. P.; Behzad, A. R.; Hooghan, B.; Sougrat, R.; Karunakaran, M.; Pradeep, N.; Vainio, U.; Peinemann, K. V. Switchable Ph-Responsive Polymeric Membranes Prepared Via Block Copolymer Micelle Assembly. *ACS Nano* **2011**, *5*, 3516−3522.
(30) Qiu, X.; Yu, H.; Karunakaran, M.; Pradeep, N.; Nunes, S. P.; Peinemann, K.-V. Selective Separation of Similarly Sized Proteins with Tunable Nanoporous Block Copolymer Membranes. *ACS Nano* **2012**, *7*, 768−776.
(31) Marques, D. S.; Vainio, U.; Chaparro, N. M.; Calo, V. M.; Bezahd, A. R.; Pitera, J. W.; Peinemann, K. V.; Nunes, S. P. Self-Assembly in Casting Solutions of Block Copolymer Membranes. *Soft Matter* **2013**, *9*, 5557−5564.
(32) Yu, H.; Qiu, X.; Nunes, S. P.; Peinemann, K.-V. Self-Assembled Isoporous Block Copolymer Membranes with Tuned Pore Sizes. *Angew. Chem., Int. Ed.* **2014**, *53*, 10072−10076.
(33) Yang, S. Y.; Ryu, I.; Kim, H. Y.; Kim, J. K.; Jang, S. K.; Russell, T. P. Nanoporous Membranes with Ultrahigh Selectivity and Flux for the Filtration of Viruses. *Adv. Mater.* **2006**, *18*, 709−712.
(34) Yang, S. Y.; Park, J.; Yoon, J.; Ree, M.; Jang, S. K.; Kim, J. K. Virus Filtration Membranes Prepared from Nanoporous Block Copolymers with Good Dimensional Stability under High Pressures and Excellent Solvent Resistance. *Adv. Funct. Mater.* **2008**, *18*, 1371−1377.
(35) Jackson, E. A.; Hillmyer, M. A. Nanoporous Membranes Derived from Block Copolymers: From Drug Delivery to Water Filtration. *ACS Nano* **2010**, *4*, 3548−3553.
(36) Jeon, G.; Jee, M.; Yang, S. Y.; Lee, B. Y.; Jang, S. K.; Kim, J. K. Hierarchically Self-Organized Monolithic Nanoporous Membrane for Excellent Virus Enrichment. *ACS Appl. Mater. Interfaces* **2014**, *6*, 1200−1206.
(37) Ke, B. B.; Wan, L. S.; Chen, P. C.; Zhang, L. Y.; Xu, Z. K. Tunable Assembly of Nanoparticles on Patterned Porous Film. *Langmuir* **2010**, *26*, 15982−15988.
(38) Widawski, G.; Rawiso, M.; Francois, B. Self-Organized Honeycomb Morphology of Star-Polymer Polystyrene Films. *Nature* **1994**, *369*, 387−389.
(39) Bai, H.; Du, C.; Zhang, A. J.; Li, L. Breath Figure Arrays: Unconventional Fabrications, Functionalizations, and Applications. *Angew. Chem., Int. Ed.* **2013**, *52*, 12240−12255.
(40) Muñoz-Bonilla, A.; Fernández-García, M.; Rodríguez-Hernández, J. Towards Hierarchically Ordered Functional Porous Polymeric Surfaces Prepared by the Breath Figures Approach. *Prog. Polym. Sci.* **2014**, *39*, 510−554.
(41) Wan, L. S.; Zhu, L. W.; Ou, Y.; Xu, Z. K. Multiple Interfaces in Self-Assembled Breath Figures. *Chem. Commun.* **2014**, *50*, 4024−4039.
(42) Wan, L. S.; Li, Q. L.; Chen, P. C.; Xu, Z. K. Patterned Biocatalytic Films via One-Step Self-Assembly. *Chem. Commun.* **2012**, *48*, 4417−4419.
(43) Wan, L. S.; Ke, B. B.; Zhang, J.; Xu, Z. K. Pore Shape of Honeycomb-Patterned Films: Modulation and Interfacial Behavior. *J. Phys. Chem. B* **2012**, *116*, 40−47.
(44) Zhu, L. W.; Yang, W.; Ou, Y.; Wan, L. S.; Xu, Z. K. Synthesis of Polystyrene with Cyclic, Ionized and Neutralized End Groups and the Self-Assemblies Templated by Breath Figures. *Polym. Chem.* **2014**, *5*, 3666−3672.
(45) Zhu, L. W.; Ou, Y.; Wan, L. S.; Xu, Z. K. Polystyrenes with Hydrophilic End Groups: Synthesis, Characterization, and Effects on the Self-Assembly of Breath Figure Arrays. *J. Phys. Chem. B* **2014**, *118*, 845−854.
(46) Zhu, L. W.; Wu, B. H.; Wan, L. S.; Xu, Z. K. Polystyrene with Hydrophobic End Groups: Synthesis, Kinetics, Interfacial Activity, and Self-Assemblies Templated by Breath Figures. *Polym. Chem.* **2014**, *5*, 4311−4320.
(47) Zhu, L. W.; Yang, W.; Wan, L. S.; Xu, Z. K. Synthesis of Core Cross-Linked Star Polystyrene with Functional End Groups and Self-Assemblies Templated by Breath Figures. *Polym. Chem.* **2014**, *5*, 5175−5182.
(48) Govor, L. V.; Bashmakov, I. A.; Kiebooms, R.; Dyakonov, V.; Parisi, J. Self-Organized Networks Based on Conjugated Polymers. *Adv. Mater.* **2001**, *13*, 588−591.
(49) Nishikawa, T.; Ookura, R.; Nishida, J.; Arai, K.; Hayashi, J.; Kurono, N.; Sawadaishi, T.; Hara, M.; Shimomura, M. Fabrication of Honeycomb Film of an Amphiphilic Copolymer at the Air-Water Interface. *Langmuir* **2002**, *18*, 5734−5740.
(50) Hayakawa, T.; Horiuchi, S. From Angstroms to Micrometers: Self-Organized Hierarchical Structure within a Polymer Film. *Angew. Chem., Int. Ed.* **2003**, *42*, 2285−2289.
(51) Ma, H.; Cui, J.; Song, A.; Hao, J. Fabrication of Freestanding Honeycomb Films with through-Pore Structures via Air/Water Interfacial Self-Assembly. *Chem. Commun.* **2011**, *47*, 1154−1156.
(52) Cong, H.; Wang, J.; Yu, B.; Tang, J. Preparation of a Highly Permeable Ordered Porous Microfiltration Membrane of Brominated Poly(Phenylene Oxide) on an Ice Substrate by the Breath Figure Method. *Soft Matter* **2012**, *8*, 8835−8839.
(53) Yin, S. Y.; Goldovsky, Y.; Herzberg, M.; Liu, L.; Sun, H.; Zhang, Y. Y.; Meng, F. B.; Cao, X. B.; Sun, D. D.; Chen, H. Y.; Kushmaro, A.; Chen, X. D. Functional Free-Standing Graphene Honeycomb Films. *Adv. Funct. Mater.* **2013**, *23*, 2972−2978.
(54) Zhang, C.; Wang, X.; Min, K.; Lee, D.; Wei, C.; Schulhauser, H.; Gao, H. Developing Porous Honeycomb Films Using Miktoarm Star Copolymers and Exploring Their Application in Particle Separation. *Macromol. Rapid Commun.* **2014**, *35*, 221−227.
(55) Ou, Y.; Zhu, L. W.; Xiao, W. D.; Yang, H. C.; Jiang, Q. J.; Li, X.; Lu, J. G.; Wan, L. S.; Xu, Z. K. Nonlithographic Fabrication of Nanostructured Micropatterns via Breath Figures and Solution Growth. *J. Phys. Chem. C* **2014**, *118*, 4403−4409.
(56) Yan, F.; Ding, A.; Girones, M.; Lammertink, R. G.; Wessling, M.; Borger, L.; Vilsmeier, K.; Goedel, W. A. Hierarchically Structured Assembly of Polymer Microsieves, Made by a Combination of Phase Separation Micromolding and Float-Casting. *Adv. Mater.* **2012**, *24*, 1551−1557.
(57) Li, L.; Zhong, Y.; Gong, J.; Li, J.; Chen, C.; Zeng, B.; Ma, Z. Constructing Robust 3-Dimensionally Conformal Micropatterns: Vulcanization of Honeycomb Structured Polymeric Films. *Soft Matter* **2011**, *7*, 546−552.
(58) Li, L.; Zhong, Y.; Gong, J.; Li, J.; Huang, J.; Ma, Z. Fabrication of Robust Micro-Patterned Polymeric Films via Static Breath-Figure Process and Vulcanization. *J. Colloid Interface Sci.* **2011**, *354*, 758−764.
(59) Du, C.; Zhang, A.; Bai, H.; Li, L. Robust Microsieves with Excellent Solvent Resistance: Cross-Linkage of Perforated Polymer Films with Honeycomb Structure. *ACS Macro Lett.* **2013**, *2*, 27−30.
(60) Warkiani, M. E.; Chen, L. Q.; Lou, C. P.; Liu, H. B.; Zhang, R.; Gong, H. Q. Capturing and Recovering of Cryptosporidium Parvum Oocysts with Polymeric Micro-Fabricated Filter. *J. Membr. Sci.* **2011**, *369*, 560−568.
(61) Hosokawa, M.; Hayata, T.; Fukuda, Y.; Arakaki, A.; Yoshino, T.; Tanaka, T.; Matsunaga, T. Size-Selective Microcavity Array for Rapid and Efficient Detection of Circulating Tumor Cells. *Anal. Chem.* **2010**, *82*, 6629−6635.